The Astrophysical Journal, 896:122 (13pp), 2020 June 20 https://doi.org/10.3847/1538-4357/ab952d


# The BAT AGN Spectroscopic Survey. XVIII. Searching for Supermassive Black Hole Binaries in X-Rays

Tingting Liu[1], Michael Koss[2], Laura Blecha[3], Claudio Ricci[4,5,6], Benny Trakhtenbrot[7], Richard Mushotzky[8], Fiona Harrison[9], Kohei Ichikawa[10], Darshan Kakkad[11], Kyuseok Oh[12], Meredith Powell[13], George C. Privon[14,15], Kevin Schawinski[16], T. Taro Shimizu[17], Krista Lynne Smith[18,21], Daniel Stern[19], Ezequiel Treister[20], and C. Megan Urry[13]

[1] Center for Gravitation, Cosmology and Astrophysics, Department of Physics, University of Wisconsin–Milwaukee, P.O. Box 413, Milwaukee, WI 53201, USA tingtliu@uwm.edu
[2] Eureka Scientific, 2452 Delmer Street Suite 100, Oakland, CA 94602-3017, USA
[3] Department of Physics, University of Florida, Gainesville, FL, USA
[4] Núcleo de Astronomía de la Facultad de Ingeniería, Universidad Diego Portales, Santiago, Chile
[5] Kavli Institute for Astronomy and Astrophysics, Peking University, Beijing 100871, People's Republic of China
[6] George Mason University, Department of Physics & Astronomy, MS 3F3, 4400 University Drive, Fairfax, VA 22030, USA
[7] School of Physics and Astronomy, Tel Aviv University, Tel Aviv 69978, Israel
[8] Department of Astronomy, University of Maryland, College Park, MD 20742, USA
[9] Cahill Center for Astronomy and Astrophysics, California Institute of Technology, Pasadena, CA 91125, USA
[10] Frontier Research Institute for Interdisciplinary Sciences, Tohoku University, Sendai 980-8578, Japan
[11] European Southern Observatory, Karl-Schwarzschild-Str. 2, D-85748, Garching bei München, Germany
[12] Korea Astronomy & Space Science Institute, 776, Daedeokdae-ro, Yuseong-gu, Daejeon 34055, Republic of Korea
[13] Department of Physics, Yale University, P.O. Box 2018120, New Haven, CT 06520-8120, USA
[14] Department of Astronomy, University of Florida, 211 Bryant Space Sciences Center, Gainesville, FL 32611, USA
[15] National Radio Astronomy Observatory, 520 Edgemont Road, Charlottesville, VA 22903, USA
[16] Department of Physics, ETH Zurich, Wolfgang-Pauli-Strasse 27, CH-8093 Zurich, Switzerland
[17] Max-Planck-Institut für extraterrestrische Physik, Postfach 1312, D-85741, Garching, Germany
[18] KIPAC at SLAC, Stanford University, Menlo Park, CA 94025, USA
[19] Jet Propulsion Laboratory, California Institute of Technology, 4800 Oak Grove Drive, MS 169-224, Pasadena, CA 91109, USA
[20] Instituto de Astrofísica, Facultad de Física, Pontificia Universidad Católica de Chile, Casilla 306, Santiago 22, Chile
*Received 2019 September 10; revised 2020 May 12; accepted 2020 May 19; published 2020 June 19*

## Abstract

Theory predicts that a supermassive black hole binary (SMBHB) could be observed as a luminous active galactic nucleus (AGN) that periodically varies on the order of its orbital timescale. In X-rays, periodic variations could be caused by mechanisms including relativistic Doppler boosting and shocks. Here we present the first systematic search for periodic AGNs using 941 hard X-ray light curves (14–195 keV) from the first 105 months of the Swift Burst Alert Telescope (BAT) survey (2004–2013). We do not find evidence for periodic AGNs in Swift-BAT, including the previously reported SMBHB candidate MCG+11−11−032. We find that the null detection is consistent with the combination of the upper-limit binary population in AGNs in our adopted model, their expected periodic variability amplitudes, and the BAT survey characteristics. We have also investigated the detectability of SMBHBs against normal AGN X-ray variability in the context of the extended ROentgen Survey with an Imaging Telescope Array (eROSITA) survey. Under our assumptions of a binary population and the periodic signals they produce, which have long periods of hundreds of days, up to 13% true periodic binaries can be robustly distinguished from normal variable AGNs with the ideal uniform sampling. However, we demonstrate that realistic eROSITA sampling is likely to be insensitive to long-period binaries because longer observing gaps reduce their detectability. In contrast, large observing gaps do not diminish the prospect of detecting binaries of short, few-day periods, as 19% can be successfully recovered, the vast majority of which can be identified by the first half of the survey.

*Unified Astronomy Thesaurus concepts:* Active galaxies (17); Surveys (1671); X-ray sources (1822)

*Supporting material:* machine-readable table

## 1. Introduction

Supermassive black hole binaries (SMBHBs) are expected as the result of galaxy mergers (e.g., Begelman et al. 1980), and yet compelling evidence for close-separation SMBHBs has been elusive. Several studies in the past few years have searched for periodically varying quasars as possible SMBHBs in optical time domain surveys, and numerous candidates have been reported (Graham et al. 2015a, 2015b; Liu et al. 2015, 2016, 2019; Charisi et al. 2016). These SMBHB candidates typically have (observed) variability periods of a few hundred days or a few years. Assuming circular Keplerian orbits, their masses ($\log(M_{\rm BH}/M_{\odot}) \sim 8-10$) and periods correspond to binary separations of ∼centiparsecs to milliparsecs, which are several orders of magnitude more compact than the scale that very long baseline interferometry observations are able to resolve currently (e.g., the radio galaxy 0402+379; Rodriguez et al. 2006) or in the future (Burke-Spolaor et al. 2018; D'Orazio & Loeb 2018). These searches for AGN periodicities have been motivated by hydrodynamic and magnetohydrodynamic simulations that show that accretion onto an SMBHB varies periodically on the order of the binary

[21] Einstein Fellow.

orbital timescale (e.g., MacFadyen & Milosavljević 2008; Noble et al. 2012; Shi et al. 2012; D'Orazio et al. 2013; Farris et al. 2014; Gold et al. 2014; Bowen et al. 2018, 2019); the torque exerted by the binary opens up a cavity in the disk in which the binary is embedded ("circumbinary disk"), and the gas instead crosses the gap from the inner edge of the circumbinary disk in the form of narrow streams. The gas eventually feeds the individual accretion disks formed around the black holes ("minidisks") at a rate that is modulated on the binary orbital timescale. Another possible mechanism is when the steady emission from the minidisk is relativistic Doppler boosted for a highly inclined, close-separation binary system (D'Orazio et al. 2015), which modulates the apparent flux on the binary orbital period. In both mechanisms, periodicities occur for a wide range of mass ratios ($q$) expected from major mergers; hydrodynamic variability is strongest when $q \gtrsim 0.1$, as the binary is able to create an overdensity in the inner edge of the circumbinary disk that interacts with the black holes (e.g., Farris et al. 2014). The Doppler boost model favors small mass ratios; however, even in an equal-mass binary, periodicity still manifests, since the enhancement and suppression do not cancel.

In the X-ray regime, an SMBHB may also display periodic variability. Similar to the UV/optical, X-ray emissions from the gas bound to the black holes may also experience Doppler boosting (Haiman 2017). Periodicity may also be produced by shocks, when the streams crossing the gap are flung outward by the black holes and hit the cavity wall of the circumbinary disk twice per orbit (Tang et al. 2018). When the stream joins a minidisk, it shock heats its outer edge and produces bright X-ray emission at tens to hundreds of keV by inverse Compton scattering (Roedig et al. 2014; see also Farris et al. 2015), which is also modulated on the orbital timescale.

Despite these predictions, the X-ray variability signatures of SMBHBs remain largely unexplored. Only recently was an SMBHB candidate reported by Severgnini et al. (2018) in the center of a Seyfert 2 galaxy at $z = 0.0362$: MCG+11−11−032. Its light curve[22] from the Burst Alert Telescope (BAT; Barthelmy et al. 2005) on board the Neil Gehrels Swift Observatory (Gehrels et al. 2004) was claimed to show a quasi-periodic variation with a period of about 25 months over the 123 month baseline, suggesting an orbital velocity of the putative SMBHB: $v \sim 0.06c$. Interestingly, its X-ray spectrum is best described by an absorbed power law with a reflection component plus two narrow Gaussian components for Fe K$\alpha$. While the energy of the second component is less well constrained, their separation in energy $\Delta E$ is consistent with the velocity derived from the variability period, assuming they are produced in either the minidisks or the inner region of the circumbinary disk.

Swift-BAT has been observing the hard X-ray sky in the 14–195 keV energy range since its launch. The fifth and most recent catalog (Oh et al. 2018) includes 105 months of observations from 2004 December to 2013 August and reports 1632 sources, 947 of which are unbeamed active galactic nuclei (AGNs). This is currently the largest sample of hard X-ray–selected AGNs with long temporal baselines and regular observations, and it presents a unique opportunity to study the hard X-ray variability of AGNs.

[22] The yet-unpublished data independently analyzed by the Palermo BAT team at Istituto Nazionale di Astrofisica (e.g., Segreto et al. 2010).

Previous AGN variability studies with Swift-BAT (Beckmann et al. 2007; Caballero-Garcia et al. 2012; Shimizu & Mushotzky 2013; Soldi et al. 2014) have measured the fractional flux variability, structure function, or power spectral density (PSD) of BAT AGNs and studied the correlation of variability with physical properties such as black hole mass and X-ray and bolometric luminosities, AGN type, or energy bands. However, no study has so far systematically searched for periodic variability that may be indicative of close SMBHBs at subparsec separations. Such a search would complement previous ones with ground-based, optical time domain surveys in two important aspects. First, abundant gas is funneled in during (gas-rich) galaxy mergers and thereby powers the SMBHs as luminous quasars (e.g., di Matteo et al. 2005; Hopkins et al. 2008), but the SMBHs are likely to be enshrouded by gas and dust, resulting in substantial obscuration in the optical, UV, and even soft X-ray bands (e.g., Ricci et al. 2017a). Very hard X-ray (>10 keV) photons, on the other hand, have a high penetrating power through the obscuring material with column densities upward of $10^{24}$ cm$^{-2}$ (e.g., Ricci et al. 2015; Koss et al. 2016) and can therefore potentially reveal SMBH duals and binaries that are inaccessible in the UV/optical (e.g., Koss et al. 2012; Ricci et al. 2017a; Satyapal et al. 2017; Koss et al. 2018).

Second, while previous numerical simulations of SMBHBs show that the accretion rate from the circumbinary disk onto the minidisks is periodically modulated, it may not directly translate to a periodic photon luminosity due to the buffering effect of the minidisk when its gas inflow timescale is longer than the modulation timescale (e.g., Farris et al. 2014). However, binary-modulated X-ray emission produced by shocks is immune to this effect due to the short timescale of Compton cooling compared to the orbital timescale (see also discussions in, e.g., Shi & Krolik 2016 and Krolik et al. 2019).

The ability of Swift-BAT to study the full variable X-ray sky in general and variable AGNs in particular will be unmatched until the completion of the extended ROentgen Survey with an Imaging Telescope Array (eROSITA; Merloni et al. 2012). It will be much more sensitive to (unobscured) AGNs, many of which will be visited at a high cadence as a result of its scanning strategy.

This paper has the dual goal of performing the first systematic search for periodic AGNs in the X-rays and investigating the prospects for detecting SMBHBs with eROSITA and is organized as follows. In Section 2, we search for periodic signals in the 105 month BAT catalog by first modeling the underlying normal AGN variability, which is characterized by higher variability power at lower frequencies ("red noise"). We also revisit the binary candidate MCG+11−11−032 reported by Severgnini et al. (2018). In Section 3, we investigate the detectability of periodic SMBHBs with eROSITA by first adopting a daily temporal sampling rate over the course of the survey and then proceed to investigate the effects of nonuniform sampling by inserting a gap every 6 months. We further investigate the detectability of short periods with more realistic sampling as a function of the total length of observations. We summarize our results in Section 4.

## 2. BAT AGNs

### 2.1. The 105 Month Swift-BAT Catalog

Swift-BAT has a wide field of view (FOV ∼60° × 100°) and is designed to monitor a comparatively large fraction of the sky for gamma-ray bursts (GRBs). While it is scanning the sky for

GRBs and other hard X-ray transients, BAT is also effectively performing a survey of the full sky with nearly uniform coverage, with 90% of the sky covered at the 11 Ms level over the period of 105 months, and the median $5\sigma$ sensitivity limit corresponds to $7.24 \times 10^{-12}$ erg cm$^{-2}$ s$^{-1}$ (Oh et al. 2018). By comparison, the International Gamma-Ray Astrophysics Laboratory (INTEGRAL; Ubertini et al. 2003) has primarily observed the Galactic plane with its Imager on Board the INTEGRAL Satellite (IBIS; Winkler et al. 2003) in the $17 - 100$ keV range with a shorter overall exposure time (Bird et al. 2010; Krivonos et al. 2010). NuSTAR (Harrison et al. 2013) has a superior sensitivity in the hard X-ray band ($3\sigma$ sensitivity at $10^{-14}$ erg cm$^{-2}$ s$^{-1}$ in the 10–30 keV range); however, it has a smaller FOV ($12\farcm2 \times 12\farcm2$) and mostly performs pointed observations.

Following the earlier survey catalogs (Markwardt et al. 2005; Tueller et al. 2008, 2010; Baumgartner et al. 2013), the fifth Swift-BAT catalog[23] (Oh et al. 2018) contains 1632 sources observed during the 105 months between 2004 December and 2013 August, 328 of which are newly identified sources since its last version, the 70 month catalog (Baumgartner et al. 2013). After making a blind source detection at the $4.8\sigma$ level and fitting for the source position, a cross-search using a fixed radius is made in the archive for counterparts observed by other telescopes/instruments, such as Swift-XRT, Chandra, and XMM-Newton. The X-ray sources are also searched for optical counterparts in the NED and SIMBAD databases. Sources with known types in their optical counterparts are further divided into classes, and the 105 month catalog includes 947 unbeamed AGNs, i.e., classified as Seyfert 1, Seyfert 2, or LINER based on their emission lines, as well as "unknown AGNs." A detailed description of the BAT hard X-ray survey data can be found in Oh et al. (2018) and references therein. One of the main data products is the light curves of BAT-detected sources spanning the duration of the survey. Instead of "snapshot" light curves from individual observations, the 105 month catalog presents the monthly binned light curves by adding individual snapshot images from each month of the survey and measuring the source flux from the total-band mosaic image.

Follow-up observations and studies of BAT-detected sources are actively being carried out. Among them is the BAT AGN Spectroscopic Survey[24] (BASS; Koss et al. 2017), a large effort to measure optical spectra for this hard X-ray–selected, uniquely unbiased sample of AGNs with complete estimates for black hole mass, accretion rate, and bolometric luminosity using dedicated spectroscopic observations. In addition to optical spectra, BASS also presents careful determination of the X-ray properties of BAT AGNs by combining Swift-BAT data with observations from a variety of soft X-ray telescopes (Ricci et al. 2017b). The BASS sample consists of the brightest ($L_{2-10\,\mathrm{keV}} \gtrsim 10^{42}$ erg s$^{-1}$) and the nearest (90% are at $z < 0.2$) AGNs, allowing detailed studies of nearby AGNs while serving as a benchmark for X-ray surveys of a large sample of high-redshift AGNs, such as the upcoming eROSITA and the planned spectroscopic follow-up of eROSITA-detected AGNs with SDSS-V (Kollmeier et al. 2017) and 4MOST (Merloni et al. 2019).

### 2.2. Variability Analysis

Our parent sample consists of 941 unbeamed AGNs in the 105 month catalog that are classified as Seyfert 1, Seyfert 2, or unknown AGN. Their source IDs, names, and coordinates are listed in Table 1. We first calculate the excess variance (Nandra et al. 1997; Edelson et al. 2002; Vaughan et al. 2003) for each light curve, which removes the apparent variation due to measurement errors, $\sigma_{\rm xs}^2 = S^2 - \overline{\sigma_{\rm err}^2}$, where $S^2$ is the variance of the light curve, and $\sigma_{\rm err}$ is the measurement error. To select intrinsically variable AGNs,[25] we compare their $\sigma_{\rm xs}^2$ with those of galaxy clusters, which are constant hard X-ray sources (e.g., Wik et al. 2011). We have inspected the Swift-XRT and XMM-Newton data of each cluster, in order to exclude those with contamination from variable AGNs in the BAT FOV. We have also used the detailed analysis of BAT clusters by Ajello et al. (2009; 2010). This process removed 8/26 clusters. As we show in Figure 1 (upper panel), the distribution of AGNs closely mimics that of clusters at the $\sigma_{\rm xs}^2 < 1.5 \times 10^{-7}$ level, indicating possible remaining systematic effects; above this level, the fraction of galaxy clusters declines to zero. Therefore, we use $\sigma_{\rm xs}^2 = 1.5 \times 10^{-7}$ as the variability threshold and select 220 AGNs (23% of the sample) for further analysis. We show the $\sigma_{\rm xs}^2$ values of the full sample in Table 1 and denote those that meet our variability threshold.

We have also calculated the fractional variability, which is normalized to the average flux of the source: $f_{\rm var} = (\sigma_{\rm XS}/\langle F \rangle) \times 100\%$ (Table 1). It is similar to the $S_{\rm V}$ parameter used by Soldi et al. (2014), where their $\sigma_{\rm Q}$ parameter reduces to $\sigma_{\rm XS}$ for uniform measurement errors. As we show in Figure 1 (lower panel), most AGNs in this sample are variable at the 30%–40% level on the ∼month timescale, similar to the sample from Soldi et al. (2014), although with a heavy tail for AGNs with fractional variability $\gtrsim$100%. We find that those high-variance values ($f_{\rm var} > 50\%$) tend to be associated with low count rates. Additionally, visual inspection of their light curves reveals a number of outliers; thus, we only show $f_{\rm var} \leqslant 200\%$ in Figure 1 for presentation purposes. We confirm that by using $\sigma_{\rm xs}^2$ instead of $f_{\rm var}$ as the variability threshold, we do not systematically bias against faint sources, as the mode count rates of the selected variable AGNs and those of nonvariable AGNs are both $\approx 5 \times 10^{-4}$ counts s$^{-1}$.

Since the 105 month light curves are uniformly sampled on monthly timescales, we compute the periodogram, which is defined as the modulus squared of the Fourier transform and is normalized to have units of (rms/mean)$^2$ Hz$^{-1}$. We ignore the point at the Nyquist frequency,[26] fit a simple linear function to the periodogram in log space, and estimate the power-law continuum of the power spectrum, where here we have corrected for the bias between the periodogram and the power spectrum by adding 0.25068 to the best-fit linear function (see Papadakis & Lawrence 1993; Vaughan 2005).

We confirm the goodness of fit using the Kuiper test, since the periodogram should scatter around the true PSD following a $\chi^2$ distribution with two degrees of freedom (e.g., Vaughan 2005). By the same token, a possible feature with a power below $-\ln[1 - (1 - \epsilon)^{1/n}]P(f)$ can be rejected as a spurious peak at the $(1 - \epsilon)$ level, where $\epsilon$ is the chosen false-alarm probability, and the trial factor $n$ is the number of frequency points in the range where the periodogram is fitted.

[23] https://swift.gsfc.nasa.gov/results/bs105mon/
[24] http://www.bass-survey.com
[25] We assume that all AGNs are likely intrinsically variable at some level. Here we will exclude any AGN whose observed variability is largely due to measurement uncertainties.
[26] Because the periodogram at this frequency is $\chi_1^2$-distributed (e.g., Vaughan 2005).

**Table 1**
Variability Properties of the BAT AGN Sample

| ID[a] | Name[b] | R.A.[c] | Decl.[d] | $\sigma^2_{\rm xs}$ $(10^{-7})$[e] | Variable?[f] | $f_{\rm var}$ (%)[g] | Type[h] |
|---|---|---|---|---|---|---|---|
| 1 | SWIFT J0001.0–0708 | 0.228 | −7.164 | 10.6620 | Y | 202.09 | Red |
| 2 | SWIFT J0001.6–7701 | 0.445 | −77.000 | 0.0296 | N | ⋯ | ⋯ |
| 3 | SWIFT J0002.5+0323 | 0.613 | 3.365 | 0.0000 | N | ⋯ | ⋯ |
| 4 | SWIFT J0003.3+2737 | 0.856 | 27.643 | 1.2593 | N | ⋯ | ⋯ |
| 5 | SWIFT J0005.0+7021 | 0.934 | 70.358 | 0.5252 | N | ⋯ | ⋯ |
| 6 | SWIFT J0006.2+2012 | 1.596 | 20.242 | 0.0000 | N | ⋯ | ⋯ |
| 7 | SWIFT J0009.4–0037 | 2.305 | −0.639 | 0.0000 | N | ⋯ | ⋯ |
| 10 | SWIFT J0021.2–1909 | 5.289 | −19.162 | 0.0000 | N | ⋯ | ⋯ |
| 13 | SWIFT J0025.8+6818 | 6.432 | 68.403 | 0.2152 | N | ⋯ | ⋯ |
| 14 | SWIFT J0026.5–5308 | 6.709 | −53.151 | 2.0127 | Y | 88.70 | Red |

**Notes.**
[a] Swift-BAT 105 month catalog ID.
[b] BAT name of the source.
[c] BAT R.A. of the source.
[d] BAT decl. of the source.
[e] Excess variance $\sigma^2_{\rm xs} = {\rm S}^2 - \overline{\sigma^2_{\rm err}}$. (A negative value is forced to be zero.)
[f] Whether the source is classified as intrinsically variable.
[g] Fractional variability $f_{\rm var} = (\sigma_{\rm XS}/\langle F\rangle) \times 100\%$.
[h] Whether the intrinsic variability can be characterized by red noise or white noise.
(This table is available in its entirety in machine-readable form.)

By fitting a simple linear function to the periodogram, we have assumed that the underlying red-noise power spectrum is described by a single power law in the frequency range of interest, and here we show that it is indeed a reasonable assumption. Since the break timescale of the X-ray power spectrum is found to correlate with black hole mass (McHardy et al. 2006; González-Martín & Vaughan 2012), we can use the best-fit correlation in González-Martín & Vaughan (2012) to estimate the expected break timescale[27]: $\log(T_{\rm br}) = 1.09\log(M_{\rm BH}) - 1.70$, where $T_{\rm br}$ is in units of days and $M_{\rm BH}$ is in units of $10^6\,M_\odot$. We use black hole masses from the internally released BASS DR2 (soon to be publicly available), which has a higher completion percentage for black hole mass measurements (≈90%) than the published DR1 (Koss et al. 2017). Assuming this sample is representative of all BAT AGNs, we expect the majority (>98%) to have break timescales $T_{\rm br} < 2$ months, which corresponds to frequencies that are higher than the Nyquist frequency in our BAT data (Figure 2). This is also consistent with the lack of detection of PSD breaks and the lower limit at $10^{-6}$ Hz reported by Shimizu & Mushotzky (2013).

Shimizu & Mushotzky (2013) also showed that the brightest AGNs do not become white noise–dominated until the ∼5 day timescale, and their power spectra can be well described by single power laws over the full frequency range. However, the fainter sources in our sample show evidence of white noise beginning to dominate at a much lower frequency; thus, we should only fit for the power-law continuum in the frequency range where red noise dominates in order to estimate its slope. Hence, for each of the 220 AGNs in our variable sample, we will also consider a "power law+constant" model, in addition to a single power-law fit (Section 2.4). Ideally, the constant power level should be consistent with the level of Poisson noise estimated from measurement errors, $P_{\rm N} = \frac{2\Delta T\overline{\sigma^2_{\rm err}}}{\mu^2}$ (Vaughan et al. 2003), where $\mu$ is the mean count rate and $\Delta T = 1$ month for the 105 month BAT light curve. (For example, the power spectrum of a constant X-ray source such as a galaxy cluster should be approximately flat and at a level that is consistent with $P_{\rm N}$.)

[27] Here we have assumed that there is no significant difference in the PSDs in the soft (<10 keV) and hard (>10 keV) X-ray bands (e.g., Shimizu & Mushotzky 2013).

### 2.3. MCG+11−11−032 Revisited

We first demonstrate this procedure by testing for the reported periodicity in MCG+11−11−032. Since its light curve presented by Severgnini et al. (2018) was independently analyzed by the Palermo team, we retrieved the light curve from their published Third Palermo BAT Catalog (3PBC) instead of the 105 month catalog (Figure 3). We consider the source red noise–dominated, since its power spectrum is significantly above the estimated noise level and the power-law slope is not flat after taking into account its uncertainty. In Figure 3, we measure its power spectrum in the full frequency range and are able to reject signals in the full range at the >90% level, including the putative period of 25 months ($\log[f/{\rm Hz}] = -7.8$) reported by Severgnini et al. (2018). However, we note several differences that may result in our different conclusions. First, Severgnini et al. (2018) adopted a different method, where the periodic function is only superimposed for visual purposes, and no systematic search or power spectral analysis was performed. Second, their data were independently processed and not available to us, so our comparison is not a direct one. Finally, their light curve was from the first 123 months of the survey (which has not been published), and thus robustly detecting two cycles of the signal in the 66 month 3PBC light curve is more difficult.

### 2.4. The BAT 105 month Sample: Power Spectrum Fitting

We then apply the method to the full sample of 220 variable AGNs in the 105 month data set. We first naively fit a single power law in the full frequency range and obtain the best-fit power-law slope and normalization and their uncertainties. If the slope is steeper than its uncertainty, we tentatively classify the power spectrum as "red," and it is "white" otherwise. We

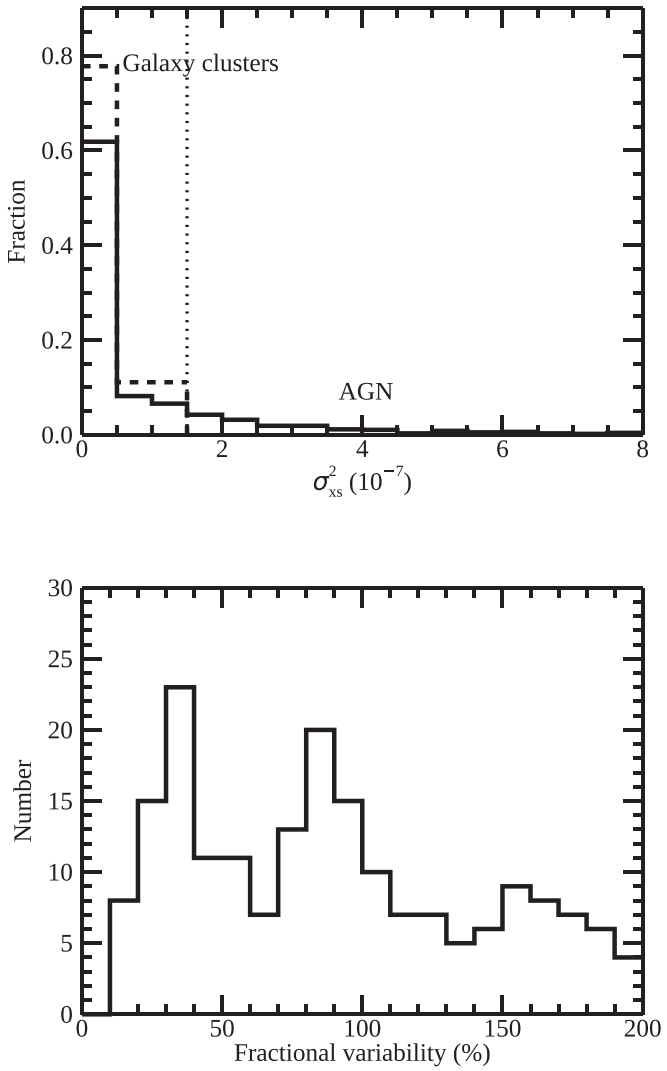


**Figure 1.** Upper panel: excess variance of the galaxy cluster sample (dashed histogram) vs. the full AGN sample (solid histogram). Those with negative excess variance are defined as $\sigma^2_{xs} = 0$. The variability threshold is marked with a dotted line. Lower panel: fractional variability distribution of the variable AGN sample. The AGNs with a fractional variability larger than 200% are defined to have $f_{var} = 200\%$ (see the text).

find that all 220 AGNs can be reasonably described by either a white power spectrum (124/220) or a red single power-law power spectrum (96/220; see Table 1).

However, for the fainter sources, the level of white noise becomes comparable to, or even dominates over, the power-law red noise at high frequencies. Hence, in cases where the estimated $P_N$ is comparable to the computed power spectrum at high frequencies, we model the power spectrum by fitting it to a power law+constant. We use the naive single power-law best-fit normalization parameter and the estimated $P_N$ level as respective initial guesses and vary by a step size of 0.1 (in logarithmic space); we vary the power-law slope in the range of [0, 3] in a step size of 0.1.

We note that since we are effectively "dereddening" the power spectrum by first fitting it to a power law and do not aim to measure the "true" PSD slope, we refrain from directly comparing our distribution of the best-fit power-law slopes with those measured by Shimizu & Mushotzky (2013), except for noting that, qualitatively, our distribution of slopes would

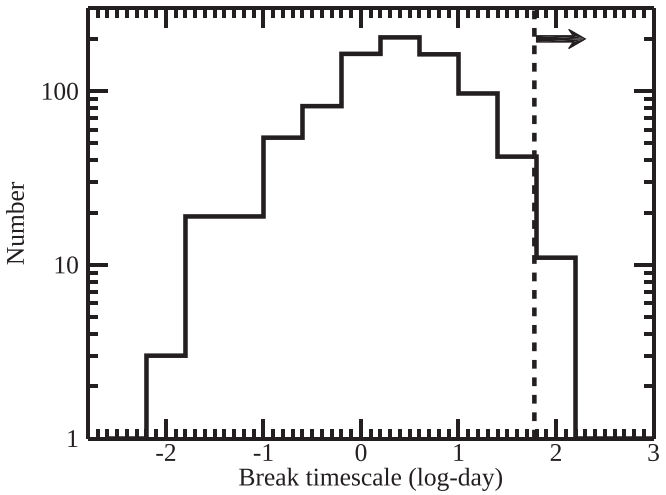


**Figure 2.** Expected PSD break timescales in units of log-day derived from the relation in González-Martín & Vaughan (2012) for the BAT AGNs with black hole mass measurements from BASS DR2. Note that the *y*-axis is log-scale for clarity. The majority (98%, or 845/861 AGNs) of break timescales are shorter than the variability timescales probed by BAT (>2 months; to the right of the dashed line).

contain more flatter slopes than the Shimizu & Mushotzky (2013) distribution, due to the high level of white noise of the fainter sources in our sample.

### 2.5. The BAT 105 month Sample: Upper Limits on Periodic Signals

After obtaining reasonable fits to the power spectra, we proceed to apply the method in Section 2.2 to test for periodic signals. We have chosen 99.7% as the significance level, since we do not expect any source in our sample to have peaks above this threshold (i.e., as a false positive). We hence reject the presence of any periodic signal at this level in this sample.

The null detection nevertheless allows us to put upper-limit constraints on periodic amplitudes in the BAT volume as a function of frequency. As we show in Figure 4, the most stringent upper limit in log-power units is given by NGC 7214 (represented by the solid line). While the periodogram is conventionally normalized to have fractional rms units, we can also calculate the variability power in terms of "absolute" units and convert to an upper limit in physical units, as the BAT count rate is normalized to the Crab ($f_{14-195\,keV} = 2.33 \times 10^{-8}$ erg cm$^{-2}$ s$^{-1}$). Hence, the best upper limit in physical flux units is provided by NGC 2110, which is also one of the brightest AGNs in the sample (dashed line in Figure 4). We note that those upper limits apply to a strictly periodic signal, rather than a "quasi-periodic" signal, which has a finite width in Fourier frequency.

Given the upper limit of ∼one periodic source per $10^4$ AGNs in optical surveys out to a higher redshift (Liu et al. 2019), a null detection in ∼1000 BAT AGNs at lower redshifts was to be expected. As we will also show in Section 3.1, the null detection in BAT is consistent with the small amplitudes of binary-induced periodic variability and the large measurement uncertainties of BAT.

Finally, we note that another previously reported SMBHB candidate, PKS 1302–102 (or PG 1302–102; hereafter PG 1302), which is also a BAT AGN was not recovered in our periodicity search. The object PG 1302 was proposed as a binary candidate for its smooth, sinusoid-like variation in the

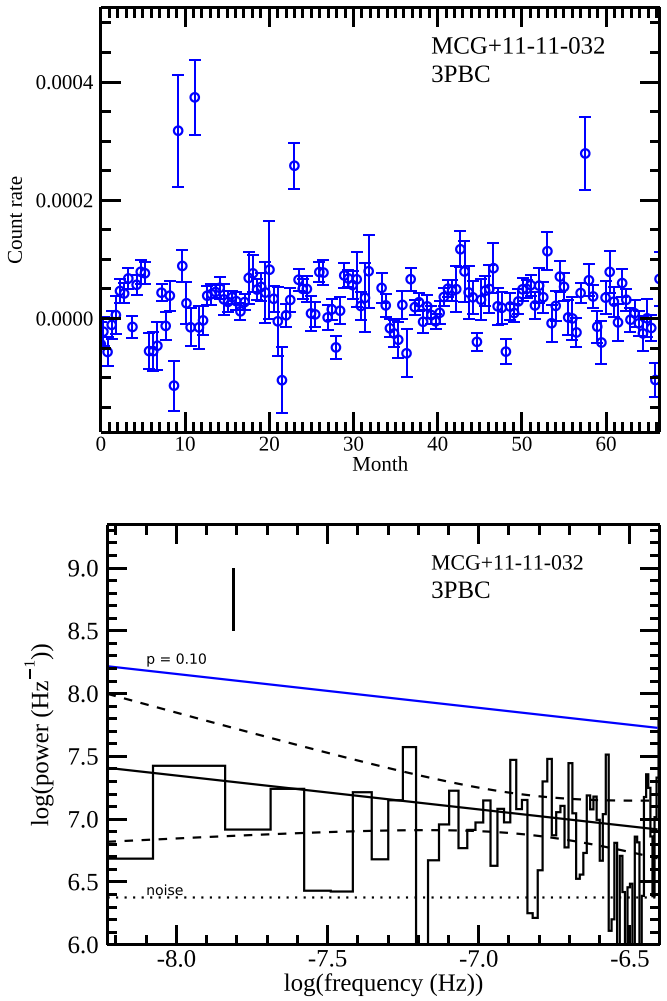


**Figure 3.** Upper panel: BAT light curve of MCG+11−11−032 since the beginning of the mission (month = 0). The 3PBC publishes light curves from the first 66 months of the survey. Lower panel: its power spectrum. The solid line represents the best-fit power-law continuum, and dashed lines represent model uncertainties, which are determined from the propagation of the uncertainties of the power-law slope and normalization and their covariance (see Vaughan 2005). The estimated noise level is marked with a dotted line. There is no peak at 25 months (black tick mark), even at the modest 90% level (blue solid line). The four outlying points in the upper panel were not removed in our analysis.

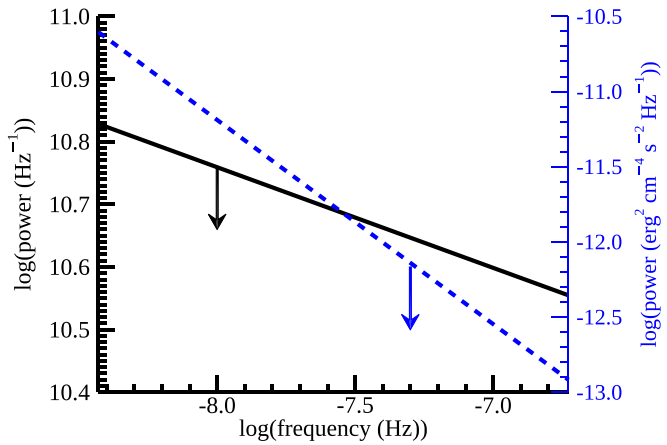


**Figure 4.** The 99.7% upper limit on a periodic signal determined from the two best sources in the BAT AGN sample, represented here in fractional rms and flux units (black solid and blue dashed lines, respectively). The significance levels are computed based on the best power spectrum fit (see the text for details).

optical light curve with an ∼5 yr observed period over ∼two cycles (Graham et al. 2015a), which was attributed to the relativistic Doppler boost from an unequal-mass binary (D'Orazio et al. 2015; however, see Vaughan et al. 2016 and Liu et al. 2018; see also Duffell et al. 2019 for an alternative interpretation). Since PG 1302, which is classified as a "beamed AGN" in the BAT 105 month catalog, was not included our parent sample, we have performed our light-curve analysis separately on this source. We find that its power spectrum shows no evidence for peaks or features and is well characterized by white noise that is consistent with the expected Poisson noise level.

## 3. Detection Prospects for eROSITA

While we do not find periodicities in the BAT sample, the eROSITA mission is likely to transform the search for SMBHBs in the X-rays, thanks to its high sensitivity in the 0.5–10 keV band and its all-sky scanning strategy. In this section, we will attempt to investigate the detectability of SMBHBs as periodic AGNs with eROSITA.

More specifically, we will test for periodic signals produced by a mock population of binaries that are superimposed on red noise. Assuming a fixed variance for the red-noise PSD (see Section 2.2 and discussions below), only two parameters are needed to generate a light curve: the amplitude and period of the signal. These two elements will then be determined by binary parameters from the mock population. While the eROSITA sky is divided in half between the German and Russian consortia, we refer to a full-sky SMBHB population whenever applicable.

### 3.1. A Mock SMBHB Sample

As it is located at the L2 Lagrangian point and scans the sky in great circles, eROSITA completes one circle in 4 hr. As its survey plane progresses around the Sun by $\sim 1^\circ$ day$^{-1}$, eROSITA completes a scan of the full sky every 6 months and eight full-sky scans during its survey lifetime (eRASS1—eRASS8). As a result of this scanning strategy, the ecliptic poles are more frequently visited than lower latitudes (more details can be found in Merloni et al. 2012). Its observing cadence in this region of the sky, combined with the survey sensitivity, could probe a wide range of variability timescales and thus possible binary parameters.

To investigate this prospect, we first construct a full-sky binary population. We adopt the mock eROSITA AGN catalog of Comparat et al. (2019). The method populates dark matter halos with galaxy stellar masses and then AGNs using an abundance-matching technique and reproduces the observed AGN X-ray luminosity function. For the remainder of this section, we adopt the full mock catalog (eRASS8), which includes 2.6 million AGNs at $0 < z < 6$. To convert the galaxy stellar mass to the black hole mass, we use the $M_{\rm stellar}$–$M_{\rm BH}$ relation from Reines & Volonteri (2015),[28] $\log(M_{\rm BH}/M_\odot) = 7.45 + 1.05\log(M_{\rm stellar}/10^{11}M_\odot)$, and the resulting range of $M_{\rm BH}$ is $\sim 10^6$–$10^8$ $M_\odot$ (we will further discuss this scaling relation and our black hole masses below).

For this study, we only focus on those AGNs near the ecliptic poles that are better sampled than those at lower latitudes. We choose areas that are no more than 2° away from

[28] Here we have not considered the possible redshift evolution of the $M_{\rm stellar}$–$M_{\rm BH}$ relation.

the poles and select AGNs from the Comparat et al. (2019) catalog that are in those regions using a grid: $\Delta$R.A. = 0.05 hr and $\Delta$decl. = 0.°5. Our parent sample contains $\sim 6 \times 10^3$ AGNs.

To compute an upper limit on the number of SMBHBs that could exist in this AGN sample, we assume a one-to-one correspondence between an AGN and an SMBHB. This is motivated by the match between the AGN lifetime of $t_{\rm AGN} \sim 10^7$ yr and the timescale for a binary to evolve from the outer edge of the circumbinary disk to coalescence (Haiman et al. 2009). We further assume that (1) all binaries in the footprint have evolved into the gravitational wave–emitting regime where the time ("residence time") a binary spends at an orbit that corresponds to the orbital timescale $t_{\rm orb}$ is $t_{\rm res} = 1.11 \times 10^7$ yr $q_s^{-1} M_7^{-5/3} t_{\rm orb}^{8/3}$ (Haiman et al. 2009), where $q_s = 4q/(1+q)^2$ with $q = M_2/M_1$ being the mass ratio, $M_7 = M_{\rm BH}/10^7\ M_\odot$, and $t_{\rm orb}$ is in units of yr; and (2) the residence timescales being probed are $t_{\rm res} = [10^5,\ 10^7]$, and each binary is assigned a residence time according to the linear dependence of the binary number rate on $t_{\rm res}$: $f(t_{\rm res}) = t_{\rm res}/t_{\rm AGN}$ (Haiman et al. 2009). The upper bound of $10^7$ yr is motivated by the binary evolution timescale, as we previously discussed, above which the binaries can no longer be active as AGNs during their entire lifetimes, and our assumptions are no longer valid. The lower bound is such that the expected number of binaries with the shortest $t_{\rm res}$ is at least a few in a sample of $10^3$–$10^4$ AGNs. While in principle, the absolute lower limit on $t_{\rm res}$ is where the separation $a = r_{\rm ISCO}$, we note that our results should be insensitive to the lower bound on $t_{\rm res}$, since binaries with very short residence timescales are exceedingly rare.

We then "sample" this binary population by considering three elements: temporal constraints, flux limit of the survey, and column density of the AGN. Since $t_{\rm res} = t_{\rm res}(t_{\rm orb}, M_{\rm BH}, q)$, we are able to calculate $t_{\rm orb}$ and therefore the observed variability timescale of each mock binary: $t_{\rm var} = t_{\rm orb}(1+z)$. Here we assume $q = 0.1$, as it strikes a balance between the mass ratio expected in a major merger and the one that can cause strong periodic modulations. We then only consider those with $t_{\rm var}$ that can be probed with the data length and sampling, i.e., $t_{\rm var} = [2,\ 730]$ days, where $t_{\rm var,\ max}$ is based on the assumption that at least two cycles are needed for periodicity detection, and $t_{\rm var,\ min}$ is determined by the cadence (see Section 3.3). Next, we impose a soft X-ray band flux limit at $4.4 \times 10^{-14}$ erg s$^{-1}$ cm$^{-2}$ (Merloni et al. 2012). Finally, we only consider column densities $N_{\rm H} < 10^{23}$ cm$^{-2}$, to which the soft X-ray band is sensitive. A total of 64 binaries met these criteria. As we show in Figure 5, their black hole mass distribution strongly peaks at $10^{7\text{–}7.5}\ M_\odot$. We also find that while this sample probes the full range of input periods, longer periods between $\sim$400 and 600 days are overall preferred.

We note a few caveats associated with our binary population. First, the $M_{\rm stellar}$–$M_{\rm BH}$ relation from Reines & Volonteri (2015) is systematically below that of elliptical galaxies and galaxies with classical bulges, and given the strong mass dependence of the binary residence time, our final mock binary population is also dependent on our particular $M_{\rm BH}$ prescription. If an $M_{\rm stellar}$–$M_{\rm BH}$ relation for ellipticals is adopted instead, so that $\log(M_{\rm BH}/M_\odot) = 8.95 + 1.04\log(M_{\rm stellar}/10^{11} M_\odot)$ (Reines & Volonteri 2015), the number of observable binaries decreases by a factor of $\sim$10, due to the shorter time for a binary to evolve through the observable timescales. Additionally, since the true $M_{\rm stellar}$–$M_{\rm BH}$ relation for AGNs is still an active area of inquiry, the aforementioned decrease is likely only a conservative estimate. Second, we have assumed that the binary evolution is primarily gravitational wave–driven, so that the residence time has a simple power-law dependence on the orbital period ($\alpha = 8/3$). However, in general, $\alpha$ is dependent on the physical mechanism driving the binary evolution, and $\alpha < 8/3$ for other processes, such as gas interaction (Haiman et al. 2009). However, those mechanisms are beyond the scope of this work.

### 3.2. Periodic Variability Properties

To calculate the expected periodic variability amplitude of each AGN, we first consider the relativistic Doppler boost model (D'Orazio et al. 2015). In this model, the line-of-sight velocity of the black hole directly translates to an apparent fractional flux variability of its minidisk emission,[29] $\Delta f/f = (3-\alpha)(v_2/c)\sin(i)$, where we adopt $\alpha = 1$ as the spectral index in the X-ray band (or a photon index of $\Gamma = 2$); $v_2$ is the velocity of the secondary black hole, $v_2 = (2\pi/1+q)(GM/4\pi^2 P)^{1/3}$; and we assume random orientations of the binaries on the sky.

In the right panel of Figure 5, we show the resulting distribution of the variability amplitudes. We find that the periodic signals produced by this sample of binaries due to Doppler boost are at the modest level of a few percent, where only $\sim$20% of the SMBHBs vary at the >5% level. It can also be seen that the distribution slightly increases toward large amplitudes, but none at the >6% level are produced by this sample.

While Doppler boosting is inevitable regardless of the details of the emission, it is expected to give only a conservative estimate of the number of detectable binaries due to its strong dependence on binary parameters and the orbital inclination. Thus, we will also consider a second periodic variability model in the following section, where we assume $f_{\rm var} = 10\%$ as an optimistic case. While this variability amplitude is higher than the highest amplitude of the Doppler-boosted periodic binaries in our sample, it may be more consistent with an alternative mechanism that could produce X-ray periodicity due to the outflung gas hitting the cavity wall (see Tang et al. 2018). Unlike Doppler boosting, the periodic amplitude in this model cannot be calculated analytically; thus, we will fix $f_{\rm var}$ at 10% for all binary parameters and inclination angles. However, we will adopt the same $t_{\rm var}$ distribution, since it is the output of the same binary population.

Working under the same upper-limit assumption of a one-to-one correspondence between an SMBHB and an AGN in the BAT volume, we also revisited the null detection of periodic AGNs with BAT by adopting the black hole mass and redshift measurements from BASS DR2. While BAT spans a baseline that is at least twice as long (and thus samples a wider range of $t_{\rm var}$), its measurement uncertainty is much larger than the fractional periodic variability ($\lesssim$8% level) of any SMBHBs, and a signal cannot be detected even without the underlying red noise. This suggests that our null detection in BAT is consistent with our chosen toy model for the (upper limit) binary population.

### 3.3. Light-curve Simulations

To investigate the detectability of a periodic signal of period $t_{\rm var}$ and amplitude $f_{\rm var}$ superimposed on red noise, we will

[29] Here we assume the emission is dominated by the secondary black hole. See Farris et al. (2014) for an accretion prescription of individual members of the binary.

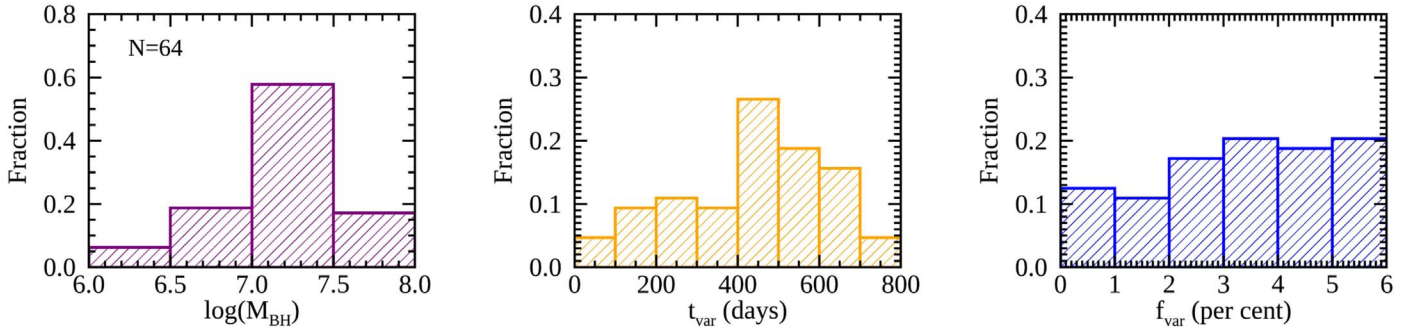


**Figure 5.** From left to right: distributions of black hole masses, variability periods, and variability amplitudes of the mock binary sample.

simulate mock light curves sampled at a given cadence. We first assume an ideal, uniform cadence that the object is visited daily for the duration of the survey. However, it should be noted that this is not the actual sampling of eRASS1—eRASS8. During each 6 month long full-sky scan, a given sky location will be paid several consecutive visits, which are separated by 4 hr, before eROSITA returns to it in the next eRASS. Since the current eROSITA scanning strategy is not yet publicly available, we have made a few assumptions about the sampling pattern: (1) the scanning law does not evolve between eRASS1 and eRASS8 and (2) a more densely sampled light curve can be rebinned to a daily cadence. A continuous and uniform sampling is expected to give us an upper-limit estimate of the detectability of periodic signals in red noise, and we will explore the erosion of detectability with uneven sampling in Section 3.5.

To produce a mock light curve of a given PSD, we use the method of Timmer & Koenig (1995). Here we again adopt a single power law, since the expected PSD break $T_{\rm br} \sim$ day is shorter than the timescales probed by the daily cadence, given the black hole masses of the sample (see Section 2.2). We draw the value of the PSD slope $\alpha$ from a normal distribution of $\mu = 0.9$ and $\sigma = 0.2$, which is consistent with previous studies of the PSD (e.g., Shimizu & Mushotzky 2013). The normalization $A$ of the single power law is such that the fractional variability is ∼30%, which is also consistent with our variable AGN sample (Section 2.2 and Figure 1) and largely independent of black hole mass (Shimizu & Mushotzky 2013). To mitigate possible spectral leakage, the parent light curve is ∼20 times longer than the duration of the survey, i.e., ∼80 yr.

Next, we inject a periodic signal, so that its period and sinusoidal amplitude are given by $t_{\rm var}$ and $f_{\rm var}$ of the mock binary, respectively. However, we only consider those with $f_{\rm var} > 5\%$ as our minimum signal-to-noise case, where the periodic signal has an amplitude of $f_{\rm var}$ as previously defined. Hence, the conservative Doppler model includes 13 periodic AGNs. We have also added Poisson noise in the light curve; we assume that the measurement uncertainty between visits is negligible compared to the intrinsic stochastic variability. This corresponds to a fractional uncertainty of ∼a few percent (see Section 2.2). We note that this fraction is likely an underestimate for the fainter sources.

Finally, we down-sample the light curve to the cadence of each mock binary to produce the final periodic AGN mock data set. To fully take into account the effect of red-noise fluctuations, we have simulated 10 realizations of this sample.

We then repeat the above light-curve simulation procedure for the optimistic case, which includes 64 AGNs. We do not require a signal-to-noise threshold in this case, since all amplitudes are fixed at 10%. We show an example light curve in the upper panel of Figure 6.

### 3.4. Detectability of Periodic AGNs with Uniform Sampling

We then apply the method in Section 2.2 and search for a periodic signal at the 98% level, which corresponds to less than one expected false positive for our sample size. We quantify the detectability with two numbers: $N_{\rm cand}$ is the number of light curves that are identified as having peaks at this level. In a systematic search where a significance level threshold is applied, they would be selected as "periodic candidates." However, most of them are false positives due to red-noise fluctuations, which is indicated by a high-significance peak located at the wrong frequency. Thus, if the injected periods are correctly identified (within a 0.1 dex uncertainty from the injected value) at the >98% level, we refer to the number of those as $N_{\rm recover}$.

We summarize the results in Table 2. Under the conservative periodic variability model, only one candidate can be identified in 5/10 realizations, but none of them are identified at the correct frequency. This is perhaps unsurprising, since the conservative case only contains 13 binaries; it also does not sample a sufficient number of binaries with large-amplitude periodic variations, making it challenging to identify them against red noise. In the optimistic case, where $f_{\rm var}$ is fixed at 10% regardless of the mock binary parameter, the recovered number has significantly increased: 5–13 periodic candidates are identified in each realization of the 64 binaries, corresponding to a candidate rate of $14.1\% \pm 3.7\%$. What is also noteworthy is the low false-positive rate of ∼10% (represented here by $1 - \frac{N_{\rm recover}}{N_{\rm cand}}$), which leads to the comparatively high recovery rate of $12.8\% \pm 3.9\%$. This may be due to the combination of large periodic amplitudes and the even sampling that we have adopted.

However, we stress that the recovery rates in both the "optimistic" and "conservative" cases should be understood as upper limits, since (1) we have assumed that each AGN being sampled hosts an SMBHB, while the actual fraction would be much lower; (2) in both cases, we have assumed that white Poisson noise is negligible with respect to red noise on the timescales of interest; (3) in our conservative case, we only consider those with large periodic amplitudes, while those with $f_{\rm var} < 5\%$ would likely be missed due to red noise, thus further lowering the overall recovery fraction; and (4) in our optimistic case, we have fixed the periodic amplitude at 10%, and it is therefore "optimistic" in the sense that the periodic amplitude is more pronounced and independent of binary parameters.

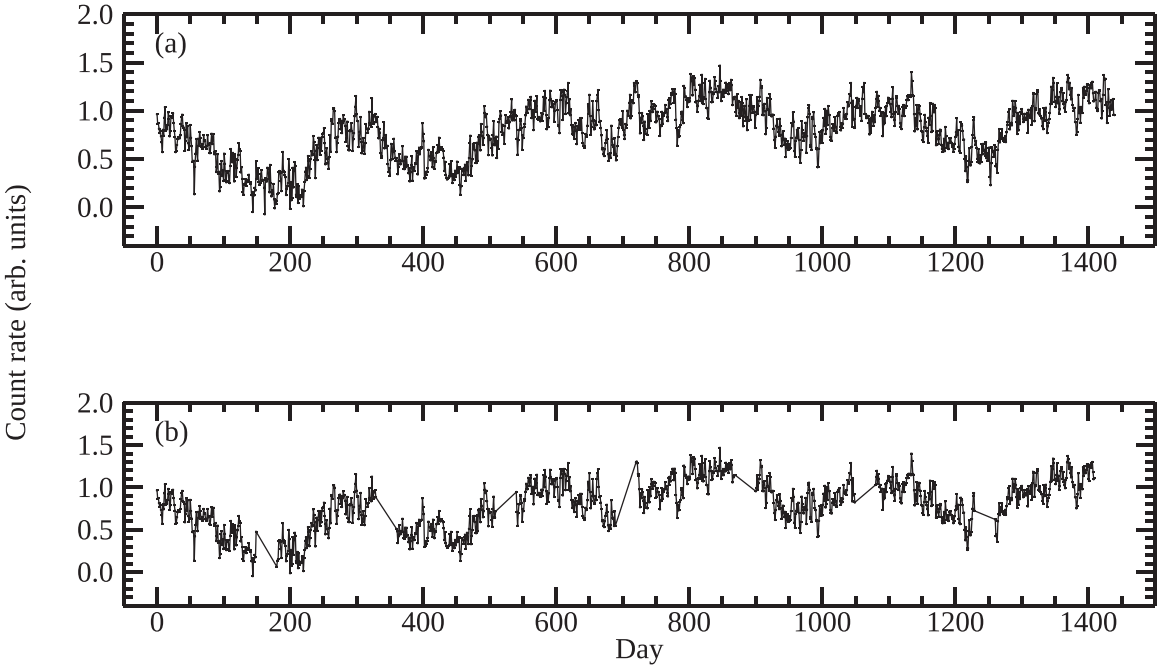


**Figure 6.** Two mock light curves down-sampled from the same parent light curve (in which a periodic signal of $P = 276$ days was injected), representing two sampling cases under consideration: (a) no gap and (b) ∼15% gap. The observation times have been normalized to the first day of observations.

**Table 2**
Number of Recovered Periodic AGNs (without Gaps)

| | Conservative | | | Optimistic | | |
|---|---|---|---|---|---|---|
| Realization | $N_{\rm tot}$ | $N_{\rm cand}$ | $N_{\rm recover}$ | $N_{\rm tot}$ | $N_{\rm cand}$ | $N_{\rm recover}$ |
| 1 | 13 | 0 | 0 | 64 | 8 | 8 |
| 2 | 13 | 1 | 0 | 64 | 11 | 9 |
| 3 | 13 | 1 | 0 | 64 | 11 | 10 |
| 4 | 13 | 0 | 0 | 64 | 7 | 6 |
| 5 | 13 | 1 | 0 | 64 | 13 | 13 |
| 6 | 13 | 0 | 0 | 64 | 10 | 9 |
| 7 | 13 | 0 | 0 | 64 | 7 | 6 |
| 8 | 13 | 1 | 0 | 64 | 9 | 8 |
| 9 | 13 | 1 | 0 | 64 | 9 | 9 |
| 10 | 13 | 0 | 0 | 64 | 5 | 4 |
| Average number | 13 | 0.5 | 0 | 64 | 9 | 8.2 |
| Average fraction | ⋯ | 3.8% | 0% | ⋯ | 14.1% | 12.8% |

We also note that our simple periodogram-based approach is only the preliminary step to reject a spurious peak at a low significance level and is not meant to claim a periodic signal at a high significance level (see Vaughan 2005). While the former is easily applicable to a large survey data set, in order to do the latter, better modeling of the underlying red noise and parameter uncertainties should be fully considered. Thus, while the Fourier method has the great advantage of speed and can be easily applied to a large (mock) survey data set, our SMBHB detectability estimates presented here are not meant to replace detailed analyses involving the actual sampling.

### *3.5. Mind the Gap: Detectability of Periodic AGNs with Nonuniform Sampling*

In fact, standard Fourier methods can no longer be used for the actual sampling of eROSITA, where consecutive visits are followed by observing gaps, the length of which is a function of the latitude of the sky location. Hence, in this section, we will investigate the effects of observing gaps on both candidate and recovery rates.

To this aim, we further down-sample the same set of simulated light curves (Section 3.3) by inserting a 1 month long gap every 6 months, which corresponds to ∼15% of the data being replaced with gaps over the full survey period. An example is shown in the lower panel of Figure 6, which is down-sampled from the same light curve in the upper panel.

Since we cannot directly apply the simple Fourier method to an unevenly sampled light curve, we fill in the missing data by linearly interpolating across the gaps. The interpolated data are then given large "measurement uncertainties" that are comparable to the standard deviation of the full light curve. We assume that by replacing only 15% of the observation length with interpolated data, any power spectrum distortion is negligible, and our method in Section 2.2 is still valid.

We repeat the period searching procedure described in Section 3.4 for light curves in the optimistic case (i.e., 10% periodic amplitude) and report the candidate and recovery rates in Table 3; 12.9% ± 4.8% of them are identified as periodic candidates, and 10.8% ± 4.3% are recovered at the correct period. We then compare these detection rates with those from Section 3.4, where the light curves are continuously and evenly sampled. As Figure 7 shows, both the number of periodic candidates and the number of recovered true periodic AGNs have decreased, which is expected due to the lack of reliable measurements during the gap periods. Further, it appears that the $N_{\rm recover}$ fraction is decreasing at a faster rate, which can be attributed to the higher number of false positives.

We hence expect that with longer gaps, the mock data set would be less sensitive to a yet wider range of variability periods, resulting in even fewer detections. In Figure 7, for visual purposes only, we extrapolate both rates to cases with longer gaps, up to a 5 month gap in a 6 month period, showing the expected further decline in the number of candidates and

**Table 3**
Number of Recovered Periodic AGNs (15% gap)

| Realization | $N_{\rm tot}$ | $N_{\rm cand}$ | $N_{\rm recover}$ |
|---|---|---|---|
| 1 | 64 | 8 | 7 |
| 2 | 64 | 10 | 9 |
| 3 | 64 | 9 | 8 |
| 4 | 64 | 6 | 4 |
| 5 | 64 | 12 | 11 |
| 6 | 64 | 9 | 7 |
| 7 | 64 | 9 | 8 |
| 8 | 64 | 8 | 7 |
| 9 | 64 | 11 | 7 |
| 10 | 64 | 1 | 1 |
| Average number | 64 | 8.3 | 6.9 |
| Average fraction | ··· | 12.9% | 10.8% |

the number of recovered periodic sources. Unfortunately, we are unable to draw reliable conclusions about the expected detectability with long gaps, since their effects on detectability would behave in a nonlinear manner for data with >15% gaps and likely render even fewer recoverable sources than the linearly extrapolated values. We hence expect that realistic eROSITA sampling, which is in the severely gappy regime, is unlikely to be sensitive to SMBHBs of periods of hundreds of days.

### 3.6. Detectability of Short Periods

However, in a case where a 5 month gap occurs every 6 months, we expect the sampling to be more sensitive to shorter timescales that can be probed with continuous sampling for ∼weeks. Hence, in this section, we will investigate the sensitivity of our sampling to short periods between 2 and 15 days. Instead of an astrophysically motivated $t_{\rm var}$ distribution, as we adopted in Section 3.1, we simply apply a uniform distribution, as our assumptions about the binary population only produce a statistically meaningful number of mock binaries with periods of hundreds of days. While our mock population no longer applies in the short-period case, many of the mechanisms that are expected to produce periodicities (Section 1) are still valid in this regime, since the black holes are expected to carry their minidisks until right before merger (e.g., Tang et al. 2018). Since the orbital period at ISCO for a nonspinning black hole of mass $10^7\ M_\odot$ is ∼1 hr, we assume that binaries of periods of days are far from the inspiral stage and that their orbits are stationary over the course of the survey.

As an optimistic estimate, we will again adopt the same fixed periodic amplitude of 10% as in Section 3.2. We then followed the same procedures as we described in Section 3.3 and generated 70 light curves for each of the 10 realizations. To search for periods, we have modified our method in Section 3.4: we split the 4 yr long light curve into eight segments, each one during which the object is observed daily for 1 month, and each segment is treated as an independent experiment. We then stack the observations by computing the average log periodogram after $N = 1, 2, ... 8$ segments, which is the analog of eRASS1–8. We further require that an object is selected as a periodic candidate or a recovered periodic source if the respective condition is met for at least two consecutive "eRASSes."

We tabulate the number of candidate and recovered periods in Table 4: 26.7% ± 4.9% of the simulations are identified as

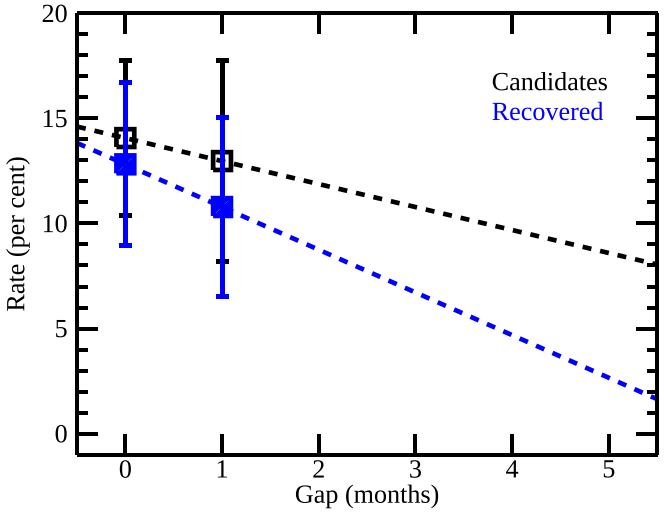


**Figure 7.** We show the candidate and recovery rates (open black and filled blue squares, respectively) vs. the length of the gap per 6 month period. The error bars represent the standard deviations of the realizations. To guide the eye, the dashed lines show the trend of decreasing rates with longer gap lengths. We note that while this trend has been linearly extrapolated to longer gaps to show the expected further decline in detectability, it does not depict the predicted candidate or recovery fraction.

**Table 4**
Number of Recovered Periodic AGNs (Short Periods)

| Realization | $N_{\rm tot}$ | $N_{\rm cand}$ | $N_{\rm recover}$ |
|---|---|---|---|
| 1 | 70 | 17 | 9 |
| 2 | 70 | 20 | 15 |
| 3 | 70 | 14 | 9 |
| 4 | 70 | 22 | 15 |
| 5 | 70 | 18 | 14 |
| 6 | 70 | 17 | 15 |
| 7 | 70 | 17 | 14 |
| 8 | 70 | 23 | 11 |
| 9 | 70 | 15 | 12 |
| 10 | 70 | 24 | 16 |
| Average number | 70 | 18.7 | 13 |
| Average fraction | ··· | 26.7% | 18.6% |

periodic candidates, and 18.6% ± 3.7% are recovered at the correct period, or a total number of $N_{\rm recover} = 130$. Both rates are higher than those for long periods (Tables 2 and 3); this is likely due to the larger number of cycles for which the periodic source is observed, which improves the chance of robustly detecting the signal against red noise.

Of the 130 recovered sources, approximately 70% are recovered by the end of eRASS2, while the remaining sources are recovered as more segments are stacked (Figure 8, upper panel). This is consistent with the expectation that a true periodic feature persists and its signal-to-noise ratio gradually improves with more observations (e.g., Liu et al. 2018). A similar approach has also been applied in the search for QPO features to ensure the signal is stable and not due to a small number of spurious observations (e.g., Pasham et al. 2014). We further find that shorter periods between 3 and 6 days are preferentially recovered (Figure 8, lower panel). In addition to the large number of cycles for which they are observed, this is also expected, since the red-noise level is lower at shorter

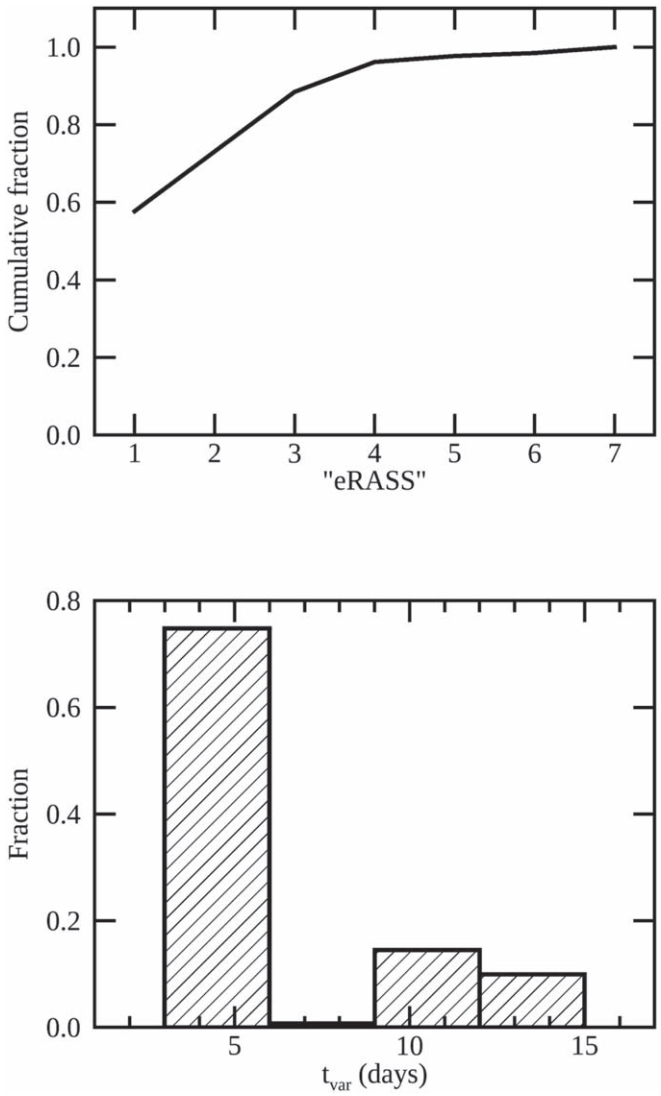


**Figure 8.** Upper panel: cumulative fraction of periods recovered as a function of eRASS. About 70% of the signals can be recovered by the end of eRASS2 at the earliest. By construction, a signal is recovered in eRASS7 at the latest (see the text). Lower panel: distribution of the recovered periods. Shorter periods are preferentially recovered due to the combination of the red-noise characteristic and the total number of observed cycles.

timescales, making it less challenging to detect a signal of the same amplitude.

### 3.7. Comparison with Previous Work

The electromagnetic detectability of SMBHBs has been investigated by several previous works. Kelley et al. (2019) used a population of binaries from the Illustris hydrodynamical cosmological simulation and prescribed periodic variability amplitudes based on the hydrodynamical simulations by Farris et al. (2014) or Doppler boost (D'Orazio et al. 2015). They found that a current all-sky survey with a magnitude limit of ∼20 mag is already capable of detecting a few binaries as hydrodynamical periodic AGNs. More encouragingly, they predicted that the Large Synoptic Survey Telescope[30] (LSST; Ivezic et al. 2019) can potentially discover more than 100 periodic AGNs as SMBHBs due to either mechanism, thanks to the much larger volume that it will probe. However, the effect of the underlying red noise, which would strongly prohibit us from detecting the periodicity, has not been explored in that work.

The recent work by Krolik et al. (2019) investigated the detectability of SMBHBs as a result of either a spectral notch in the UV/optical band due to the cavity in the circumbinary disk or an enhancement in the hard X-rays as the accretion streams shock heat the minidisks (Roedig et al. 2014). Using a population of binaries similarly "formed" in a cosmological simulation, they predicted that there could be ∼100 binaries with X-ray flux $>10^{-13}$ erg s$^{-1}$ cm$^{-2}$ under either model, and X-ray-enhanced binaries are a factor of a few more observable than binaries with the spectral notch feature. While the hard X-ray enhancement should also vary periodically, as we discussed in Section 1, identifying such a signature is also susceptible to red noise, since the Compton reflection spectrum in the hard X-ray band should also vary in a stochastic fashion in response to the continuum.

Using an observationally based approach, Liu et al. (2019) adopted a quasar luminosity function and an empirical variability amplitude–luminosity relation and "selected" variable quasars using the same pipeline as the one applied to their systematic search in the Pan-STARRS1 (Kaiser et al. 2010; Chambers et al. 2016) Medium Deep Survey (PS1 MDS) and converted their upper limit from PS1 MDS to a rate for LSST: $N_{\rm LSST} < 3500$. Interestingly, if the more conservative expectation value of $N_{\rm PS1\ MDS} \sim 0.06$ based on the independent predictions by Kelley et al. (2019) is adopted instead, they also arrived at a similar rate of $N_{\rm LSST} \sim 200$.

However, the effect of sampling on the periodicity detection rate was not investigated by any previous work. As we showed in Section 3.4, the high level of red noise and red-noise fluctuations hinders the effort to identify periodic signals due to their modest amplitudes; therefore, it is quite possible that of the 100–200 binaries predicted by Kelley et al. (2019) or Krolik et al. (2019), only a fraction can be identified observationally. The exact fraction is strongly dependent on the amplitude of the periodic signal, as we discussed in Section 3.4.

The prospects for detecting SMBHBs at all are nevertheless encouraging, given the large number of predicted SMBHBs identifiable by X-ray signatures. Assuming an optimistic recovery fraction of 13% (Section 3.4) and extrapolating the same fraction to the full sky, where there are ∼2000 SMBHBs with enhanced hard X-ray emissions at a few tens of keV with flux $f > 10^{-14}$ erg cm$^{-2}$ s$^{-1}$, ∼10% of which have short binary periods $P \lesssim 5$ yr (Krolik et al. 2019), we expect to detect ∼26 over 10 yr (we assume again that at least two cycles are required). This would require an all-sky hard X-ray survey with a sensitivity down to $10^{-14}$ erg cm$^{-2}$ s$^{-1}$ with a few percent uncertainty; however, the detection of an enhanced hard X-ray emission, accompanied by periodicity, would provide unambiguous evidence for an SMBHB.

## 4. Summary and Conclusions

The AGNs that host SMBHBs are predicted to vary periodically on roughly the binary orbital timescale from optical to X-rays. We have performed the first systematic search for SMBHBs in X-rays with Swift-BAT. While we do not find evidence for SMBHBs in the first 105 months of BAT data, including the previously reported SMBHB candidate

[30] It is now known as the Vera C. Rubin Observatory Legacy Survey of Space and Time.

MCG+11−11−032, we have placed an upper-limit constraint on periodic signals in the BAT volume. We further find that the lack of detections is consistent with the small expected periodic amplitudes produced by a population of SMBHBs, as well as the upper-limit detection rates inferred from previous searches in optical time domain surveys.

We have also investigated the prospects of detecting SMBHBs with eROSITA by constructing an upper-limit population model for SMBHBs and adopting prescriptions for their periodic amplitudes. We fully take into account normal AGN X-ray variability with the red-noise characteristic and investigate the detectability of those periodicities in red noise. For uniformally sampled light curves, we find that 13% of the periodic AGNs can be robustly identified against red noise, but the detection rate decreases with longer observing gaps. While we are unable to make solid predictions about the detectability with realistic eROSITA sampling based on our analysis in the short-gap regime, we speculate that it is unlikely to be sensitive to bona fide SMBHBs of hundreds-of-days periods.

By contrast, short periods of days to weeks are more detectable (19%), having benefited from more cycles being observed and the evolution of the power spectrum over time. In particular, 70% of the recovered periods are identified by eRASS2, or the first year of the survey, while the remaining ones are gradually detected as the signal builds up over the course of the full survey. Shorter periods of a few days are more likely to be detected, as expected from the combination of the total number of observed cycles and the AGN red-noise characteristic.

T.L., M.K., and G.C.P. thank the Aspen Center for Physics, which is supported by National Science Foundation grant PHY-1607611, for hosting the "Astrophysics of Massive Black Hole Mergers: From Galaxy Mergers to the Gravitational Wave Regime" workshop, where many stimulating discussions took place and this work was initiated. We thank the referee for a constructive report that helped improve the paper and Erin Kara for a helpful comment.

T.L. is supported by NANOGrav National Science Foundation Physics Frontiers Center award No. 1430284. M.K. acknowledges support from NASA through ADAP award NNH16CT03C. L.B. acknowledges support from National Science Foundation grant AST-1715413. C.R. acknowledges support from the CONICYT+PAI Convocatoria Nacional subvencion a instalacion en la academia convocatoria año 2017 PAI77170080 and Fondecyt Iniciacion grant 11190831. K.O. acknowledges support from the National Research Foundation of Korea (NRF-2020R1C1C1005462). E.T. acknowledges support from CONICYT-Chile grants Basal-CATA AFB-170002, FONDECYT Regular 1160999 and 1190818, and Anillo de Ciencia y Tecnologia ACT1720033. G.C.P. acknowledges support from the University of Florida.

This research has made use of data and/or software provided by the High Energy Astrophysics Science Archive Research Center (HEASARC), which is a service of the Astrophysics Science Division at NASA/GSFC. We acknowledge the use of public data from the Swift data archive.

*Facility:* Swift(BAT).

## ORCID iDs

Tingting Liu https://orcid.org/0000-0001-5766-4287
Michael Koss https://orcid.org/0000-0002-7998-9581
Laura Blecha https://orcid.org/0000-0002-2183-1087
Claudio Ricci https://orcid.org/0000-0001-5231-2645
Benny Trakhtenbrot https://orcid.org/0000-0002-3683-7297
Richard Mushotzky https://orcid.org/0000-0002-7962-5446
Kohei Ichikawa https://orcid.org/0000-0002-4377-903X
Kyuseok Oh https://orcid.org/0000-0002-5037-951X
Meredith Powell https://orcid.org/0000-0003-2284-8603
George C. Privon https://orcid.org/0000-0003-3474-1125
Kevin Schawinski https://orcid.org/0000-0001-5464-0888
T. Taro Shimizu https://orcid.org/0000-0002-2125-4670
Krista Lynne Smith https://orcid.org/0000-0001-5785-7038
Daniel Stern https://orcid.org/0000-0003-2686-9241
Ezequiel Treister https://orcid.org/0000-0001-7568-6412
C. Megan Urry https://orcid.org/0000-0002-0745-9792

## References

Ajello, M., Rebusco, P., Cappelluti, N., et al. 2009, ApJ, 690, 367
Ajello, M., Rebusco, P., Cappelluti, N., et al. 2010, ApJ, 725, 1688
Barthelmy, S. D., Barbier, L. M., Cummings, J. R., et al. 2005, SSRv, 120, 143
Baumgartner, W. H., Tueller, J., Markwardt, C. B., et al. 2013, ApJS, 207, 19
Beckmann, V., Barthelmy, S. D., Courvoisier, T. J.-L., et al. 2007, A&A, 475, 827
Begelman, M. C., Blandford, R. D., & Rees, M. J. 1980, Natur, 287, 307
Bird, A. J., Bazzano, A., Bassani, L., et al. 2010, ApJS, 186, 1
Bowen, D. B., Mewes, V., Campanelli, M., et al. 2018, ApJL, 853, L17
Bowen, D. B., Mewes, V., Noble, S. C., et al. 2019, ApJ, 879, 76
Burke-Spolaor, S., Blecha, L., Bogdanovic, T., et al. 2018, arXiv:1808.04368
Caballero-Garcia, M. D., Papadakis, I. E., Nicastro, F., & Ajello, M. 2012, A&A, 537, A87
Chambers, K. C., Magnier, E. A., Metcalfe, N., et al. 2016, arXiv:1612.05560
Charisi, M., Bartos, I., Haiman, Z., et al. 2016, MNRAS, 463, 2145
Comparat, J., Merloni, A., Salvato, M., et al. 2019, MNRAS, 487, 2005
di Matteo, T., Springel, V., & Hernquist, L. 2005, Natur, 433, 604
D'Orazio, D. J., Haiman, Z., & MacFadyen, A. 2013, MNRAS, 436, 2997
D'Orazio, D. J., Haiman, Z., & Schiminovich, D. 2015, Natur, 525, 351
D'Orazio, D. J., & Loeb, A. 2018, ApJ, 863, 185
Duffell, P. C., D'Orazio, D., Derdzinski, A., et al. 2019, arXiv:1911.05506
Edelson, R., Turner, T. J., Pounds, K., et al. 2002, ApJ, 568, 610
Farris, B. D., Duffell, P., MacFadyen, A. I., & Haiman, Z. 2014, ApJ, 783, 134
Farris, B. D., Duffell, P., MacFadyen, A. I., & Haiman, Z. 2015, MNRAS, 446, L36
Gehrels, N., Chincarini, G., Giommi, P., et al. 2004, ApJ, 611, 1005
Gold, R., Paschalidis, V., Etienne, Z. B., Shapiro, S. L., & Pfeiffer, H. P. 2014, PhRvD, 89, 064060
González-Martín, O., & Vaughan, S. 2012, A&A, 544, A80
Graham, M. J., Djorgovski, S. G., Stern, D., et al. 2015a, Natur, 518, 74
Graham, M. J., Djorgovski, S. G., Stern, D., et al. 2015b, MNRAS, 453, 1562
Haiman, Z. 2017, PhRvD, 96, 023004
Haiman, Z., Kocsis, B., & Menou, K. 2009, ApJ, 700, 1952
Harrison, F. A., Craig, W. W., Christensen, F. E., et al. 2013, ApJ, 770, 103
Hopkins, P. F., Hernquist, L., Cox, T. J., & Kereš, D. 2008, ApJS, 175, 356
Ivezic, Z., Tyson, J. A., Abel, B., et al. 2019, ApJ, 873, 111
Kaiser, N., Burgett, W., Chambers, K., et al. 2010, Proc. SPIE, 7733, 77330E
Kelley, L. Z., Haiman, Z., Sesana, A., & Hernquist, L. 2019, MNRAS, 485, 1579
Kollmeier, J. A., Zasowski, G., Rix, H.-W., et al. 2017, arXiv:1711.03234
Koss, M., Mushotzky, R., Treister, E., et al. 2012, ApJL, 746, L22
Koss, M., Trakhtenbrot, B., Ricci, C., et al. 2017, ApJ, 850, 74
Koss, M. J., Assef, R., Baloković, M., et al. 2016, ApJ, 825, 85
Koss, M. J., Blecha, L., Bernhard, P., et al. 2018, Natur, 563, 214
Krivonos, R., Tsygankov, S., Revnivtsev, M., et al. 2010, A&A, 523, A61
Krolik, J. H., Volonteri, M., Dubois, Y., & Devriendt, J. 2019, ApJ, 879, 110
Liu, T., Gezari, S., Ayers, M., et al. 2019, ApJ, 884, 36
Liu, T., Gezari, S., Burgett, W., et al. 2016, ApJ, 833, 6
Liu, T., Gezari, S., Heinis, S., et al. 2015, ApJL, 803, L16
Liu, T., Gezari, S., & Miller, M. C. 2018, ApJL, 859, L12
MacFadyen, A. I., & Milosavljević, M. 2008, ApJ, 672, 83
Markwardt, C. B., Tueller, J., Skinner, G. K., et al. 2005, ApJL, 633, L77
McHardy, I. M., Koerding, E., Knigge, C., Uttley, P., & Fender, R. P. 2006, Natur, 444, 730
Merloni, A., Alexander, D. A., Banerji, M., et al. 2019, Msngr, 175, 42

Merloni, A., Predehl, P., Becker, W., et al. 2012, arXiv:1209.3114
Nandra, K., George, I. M., Mushotzky, R. F., Turner, T. J., & Yaqoob, T. 1997, ApJ, 476, 70
Noble, S. C., Mundim, B. C., Nakano, H., et al. 2012, ApJ, 755, 51
Oh, K., Koss, M., Markwardt, C. B., et al. 2018, ApJS, 235, 4
Papadakis, I. E., & Lawrence, A. 1993, MNRAS, 261, 612
Pasham, D. R., Strohmayer, T. E., & Mushotzky, R. F. 2014, Natur, 513, 74
Reines, A. E., & Volonteri, M. 2015, ApJ, 813, 82
Ricci, C., Bauer, F. E., Treister, E., et al. 2017a, MNRAS, 468, 1273
Ricci, C., Trakhtenbrot, B., Koss, M. J., et al. 2017b, ApJS, 233, 17
Ricci, C., Ueda, Y., Koss, M. J., et al. 2015, ApJL, 815, L13
Rodriguez, C., Taylor, G. B., Zavala, R. T., et al. 2006, ApJ, 646, 49
Roedig, C., Krolik, J. H., & Miller, M. C. 2014, ApJ, 785, 115
Satyapal, S., Secrest, N. J., Ricci, C., et al. 2017, ApJ, 848, 126
Segreto, A., Cusumano, G., Ferrigno, C., et al. 2010, A&A, 510, A47
Severgnini, P., Cicone, C., della Ceca, R., et al. 2018, MNRAS, 479, 3804
Shi, J.-M., & Krolik, J. H. 2016, ApJ, 832, 22
Shi, J.-M., Krolik, J. H., Lubow, S. H., & Hawley, J. F. 2012, ApJ, 749, 118
Shimizu, T. T., & Mushotzky, R. F. 2013, ApJ, 770, 60
Soldi, S., Beckmann, V., Baumgartner, W. H., et al. 2014, A&A, 563, A57
Tang, Y., Haiman, Z., & MacFadyen, A. 2018, MNRAS, 476, 2249
Timmer, J., & Koenig, M. 1995, A&A, 300, 707
Tueller, J., Baumgartner, W. H., Markwardt, C. B., et al. 2010, ApJS, 186, 378
Tueller, J., Mushotzky, R. F., Barthelmy, S., et al. 2008, ApJ, 681, 113
Ubertini, P., Lebrun, F., di Cocco, G., et al. 2003, A&A, 411, L131
Vaughan, S. 2005, A&A, 431, 391
Vaughan, S., Edelson, R., Warwick, R. S., & Uttley, P. 2003, MNRAS, 345, 1271
Vaughan, S., Uttley, P., Markowitz, A. G., et al. 2016, MNRAS, 461, 3145
Wik, D. R., Sarazin, C. L., Finoguenov, A., et al. 2011, ApJ, 727, 119
Winkler, C., Courvoisier, T. J.-L., di Cocco, G., et al. 2003, A&A, 411, L1